ChemComm

COMMUNICATION

View Article Online
View Journal | View Issue



Cite this: *Chem. Commun.*, 2022, **58**, 10091

Received 19th July 2022,
Accepted 9th August 2022

DOI: 10.1039/d2cc04028j

rsc.li/chemcomm



# Isolating elusive 'Al(μ-O)M' intermediates in $CO_2$ reduction by bimetallic Al–M complexes (M = Zn, Mg)†

Matthew J. Evans,[a] George H. Iliffe,[a] Samuel E. Neale,[b] Claire L. McMullin,*[b] J. Robin Fulton,[a] Mathew D. Anker[a] and Martyn P. Coles*[a]

**The reaction of compounds containing Al–Mg and Al–Zn bonds with $N_2O$ enabled isolation of the corresponding Al(μ-O)M complexes. Electronic structure analysis identified largely ionic Al–O and O–M bonds, featuring an anionic μ-oxo centre. Reaction with $CO_2$ confirmed that these species correspond to the proposed intermediates in the formation of μ-carbonate compounds.**

The synergistic combination of metal centres in a bimetallic complex can promote reactivity that is divergent from their monomeric counterparts.[1] This effect is amplified in complexes containing direct metal–metal bonds,[2] with early-late heterobimetallic compounds of the transition elements playing a central role in this field.[3] As the main contributor to global warming, the transformation of carbon dioxide into value-added products has important societal benefits,[4] and its two electron reduction *via* insertion into metal–metal bonds offers an attractive entry towards achieving this goal.[5]

Heterobimetallic complexes featuring polarised Al–**M** bonds have demonstrated the facile activation of $CO_2$. This has been aided by the discovery of aluminyl anions,[6] with systems supported by $[4,5\text{-(NDipp)}_2\text{-}2,7\text{-}t\text{Bu}_2\text{-}9,9\text{-Me}_2\text{-xanthene}]^{2-}$ ($_{xanth}NON^{Dipp}$),[7] and $[(CH_2SiMe_2NDipp)_2]^{2-}$ ($NC_2N^{Dipp}$)[8] ligands dominant in this field (Fig. 1). The aluminium fragments have been partnered with Zn,[9] and the coinage metals (Cu, Ag, Au)[10] to afford complexes containing unsupported Al–**M** bonds (**I**). Reaction of **I** with $CO_2$ proceeds with insertion into the Al–**M** bond to afford the corresponding dioxocarbene (**II**), the mechanism of which has been studied computationally.[10c,d] Species **II** can react with additional $CO_2$ to afford the carbonate, **IV**, believed to proceed *via* an intermediate μ-oxo species **III** formed by the extrusion of CO. Examples of this putative intermediate have yet to be isolated in these systems, although other compounds containing the Al(μ-O)**M** motif have demonstrated this reactivity.[11] We report herein the synthesis of Al–**M** (**M** = Zn, Mg) complexes derived from the $[Al(NON^{Dipp})]^-$ aluminyl ($NON^{Dipp}$ = $[O(SiMe_2NDipp)_2]^{2-}$),[12] and their reactivity with $CO_2$, including isolation of the first μ-oxo intermediates (**III**). Although we acknowledge obvious differences in the chemistry of Mg and Zn compared with Cu, Ag and Au, we feel that the results presented here support the validity of the postulated mechanism of carbonate formation in the previously studied systems.

The reaction of $[K\{Al(NON^{Dipp})\}]_2$ with two equivalents of $Mg(BDI^{Mes})I(OEt_2)$ or $Zn(BDI^{Mes})(\mu\text{-Cl})_2Li(THF)_2$ afforded the bimetallic complexes $(NON^{Dipp})Al\text{–}M(BDI^{Mes})$ (**1-M**, Scheme 1). The $^1H$ NMR spectra showed the expected peaks for the

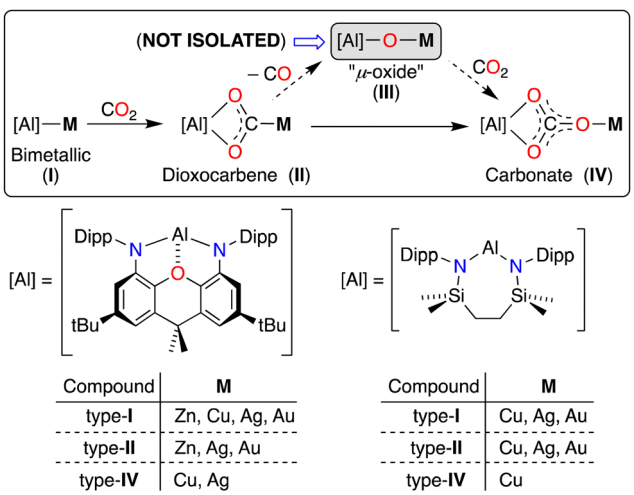


| Compound | M |
|---|---|
| type-I | Zn, Cu, Ag, Au |
| type-II | Zn, Ag, Au |
| type-IV | Cu, Ag |

| Compound | M |
|---|---|
| type-I | Cu, Ag, Au |
| type-II | Cu, Ag, Au |
| type-IV | Cu |

Fig. 1 Aluminyl derived Al–**M** systems that activate of $CO_2$. Dipp = 2,6-$i\text{Pr}_2C_6H_3$.

[a] *School of Chemical and Physical Sciences, Victoria University of Wellington, P.O. Box 600, Kelburn, Wellington, 6012, New Zealand. E-mail: martyn.coles@vuw.ac.nz*
[b] *Department of Chemistry, University of Bath, Bath, BA2 7AY, UK. E-mail: cm2025@bath.ac.uk*

† Electronic supplementary information (ESI) available: Experimental details and characterization data; full details of computational experiments. CCDC 2183690–2183696. For ESI and crystallographic data in CIF or other electronic format see DOI: https://doi.org/10.1039/d2cc04028j

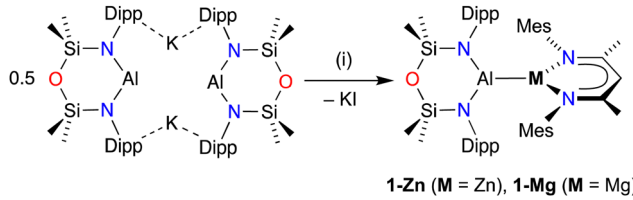


Scheme 1 Synthesis of **1-Zn** and **1-Mg**. (i) Mg(BDI$^{Mes}$)I(OEt$_2$) or [Li(THF)$_2$][Zn(BDI$^{Mes}$)Cl$_2$]. BDI$^{Mes}$ = [HC{CMeNMes}$_2$]$^-$.

(NON$^{Dipp}$)- and (BDI$^{Mes}$)-ligands in a 1 : 1 ratio, with broad resonances for the SiMe$_2$ groups in **1-Zn** suggesting restricted rotation about the Al–Zn bond. X-Ray diffraction studies show both systems crystallise as isostructural monomers containing unsupported Al–**M** bonds (Fig. 2). The Al–Zn (2.4860(5) Å) and Al–Mg (2.7711(6) Å) bonds are within the range of other reported Al–Mg (2.696(1)–2.7980(6) Å)[7,8,13] and Al–Zn (2.448(2)–2.491(1) Å)[9,13a–c,14] bonds.

DFT calculations at the BP86/BS2 level of theory (see ESI†) and subsequent NBO (Natural Bonding Orbital) analysis of **1-Zn** and **1-Mg** highlights the electronic variance between these two species. The Wiberg Bond Index (WBI) values for the Al–**M** bonds suggest single bond character, which is stronger in **1-Zn** (WBI$_{(Al–Zn)}$ = 0.740) than in **1-Mg** (WBI$_{(Al–Mg)}$ = 0.602). Interestingly, natural atomic charge data suggest a reversal in the polarity of the Al–**M** bond based on the charge difference ($\Delta q = q_{Al} - q_M$, Fig. 2), with Al more electropositive than Zn in **1-Zn** ($\Delta q$ = +0.284), whereas Mg is the more electropositive partner in **1-Mg** ($\Delta q$ = −0.396). These data contrast those calculated for ($_{xanth}$NON$^{Dipp}$)Al–**M**(BDI$^{Mes}$), which showed that Al was the less electropositive element in both Al–Mg ($\Delta q$ = −0.69) and Al–Zn ($\Delta q$ = −0.30) complexes.[9]

Further investigation of these charge differences revealed an appreciable basis set dependence on the $q_M$ values calculated for Al–**M** complexes. For example, we have performed calculations on the ($_{xanth}$NON$^{Dipp}$) system using a triple-zeta basis set approach (6-311 + +G** = BS2), which show the same polarity

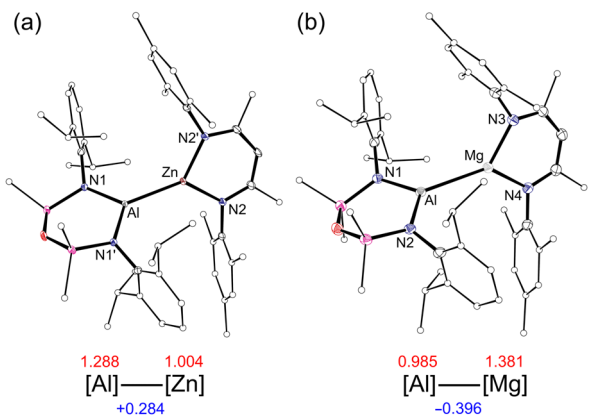


Fig. 2 Thermal displacement plot (30% probability, H-atoms omitted, selected carbon atoms represented as spheres) of (a) **1-Zn** (′ = −*x*, *y*, $\frac{1}{2}$ − *z*) and (b) **1-Mg**. Selected bond lengths (Å): (a) Al–Zn 2.4860(5); (b) Al–Mg 2.7711(6). Bottom: Natural atomic charge data for the Al and **M** atoms (red = $q_{Al}/q_M$; blue = $\Delta q = q_{Al} - q_M$) {BP86/BS2; NBO7}.

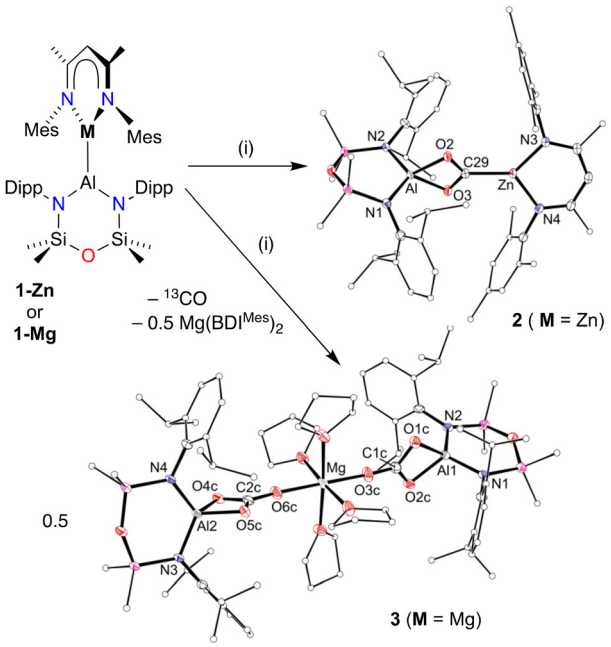


Scheme 2 Synthesis of **2** and **3**. (i) $^{13}CO_2$ (1 bar). Displacement ellipsoid plots of **3** (30% ellipsoids; H-atoms omitted; C-atoms represented as spheres). Selected bond lengths (Å) and angles (°): **2** {value from second molecule} C29–O2 1.2917(18) {1.292(2)}, C29–O3 1.2970(18) {1.2938(19)}, Al1–O2 1.8679(11) {1.8682(11)}, Al1–O3 1.8587(11) {1.8602(11)}, Zn1–C29 1.9641(14) {1.9640(15)}. **3** C1c–O1c 1.316(5), C1c–O2c 1.303(5), C1c–O3c 1.235(4), C2c–O4c 1.300(4), C2c–O5c 1.324(4), C2c–O6c 1.228(4).

direction for the Al–Mg bond as noted in **1-Mg**. However, for the Al–Zn complex, the charge imbalance and bond polarity is reversed when compared with reported values calculated at the PBE0/SVP level ($q_{Al}$ = 0.96, $q_{Zn}$ = 1.26 and $\Delta q$ = −0.30), with our results showing values of $q_{Al}$ = 1.262, $q_{Zn}$ = 1.001 giving a $\Delta q$ = +0.261 at the BP86/BS2 level.[9,15]

Exposing a solution of **1-Zn** to 1 bar of $^{13}CO_2$ afforded (NON$^{Dipp}$)Al(μ-1κ$^2$O,O′:2κC-O$_2$C)Zn(BDI$^{Mes}$) (**2**, Scheme 2). A $^{13}$C{$^1$H} resonance at $\delta_c$ 222.2 is characteristic of the carbenic carbon and reminiscent of other dioxocarbene complexes (range: $\delta_c$ 219.7[9] to $\delta_c$ 242.3[10c]). The X-ray structure confirms the expected regiochemistry of the inserted $CO_2$ and is consistent with other examples of **II**.[9,10c,d] The carbon–oxygen distances (range: 1.2917(18)–1.2970(18) Å) indicate delocalization, with relatively short Zn–C bonds.[16]

In contrast to **1-Zn**, monitoring the reaction of **1-Mg** with $^{13}CO_2$ (1 bar) at room temperature by $^{13}$C NMR spectroscopy showed the immediate appearance of a peak at $\delta_C$ 184.5 corresponding to $^{13}$CO (Fig. S17, ESI†). This mirrors the reaction of ($_{xanth}$NON$^{Dipp}$)Al–Cu(P*t*Bu$_3$) with $CO_2$, which directly formed the carbonate complex **IV** at −78 °C (Fig. 1). The $^{13}$C{$^1$H} NMR spectrum of crystals isolated from the reaction showed a $^{13}$C enriched peak at $\delta_C$ 164.1 consistent with [$^{13}CO_3$]$^{2-}$. X-Ray diffraction of the product confirmed the formation of carbonate in {(NON$^{Dipp}$)Al(μ-1κ$^2$O,O′:2κO″-CO$_3$)}$_2${Mg(THF)$_4$} (**3**, Scheme 2).

Each aluminium is O,O′-coordinated to a planar [CO$_3$]$^{2-}$ ligand. The remaining oxygen atom of each carbonate is *trans*-bound to an octahedral magnesium, with four molecules of

THF completing the coordination sphere. A plausible rationale for this result is that the reaction proceeds *via* the monocarbonate (NON$^{Dipp}$)Al(CO$_3$)Mg(BDI$^{Mes}$), which exists in a Schlenk-type equilibrium with **3** and Mg(BDI$^{Mes}$)$_2$,[17] although we were unable to isolate the homoleptic magnesium product in this study.

Previous work with potassium aluminyl systems identified that formation of carbonate compounds from $CO_2$ proceeded *via* monoalumoxane anions containing terminal Al–O bonds.[18] These species were isolated as [Al($_{xanth}$NON$^{Dipp}$)(O)]$^-$ and [Al(NON$^{Dipp}$)(O)]$^-$ from the reaction of the corresponding potassium aluminyl with $N_2O$ gas. Analogous compounds have been inferred as intermediates in the conversion of $CO_2$ to carbonate in bimetallic Al–**M** (**M** = Cu, Ag, Au) systems (**III**, Fig. 1), although no examples have been isolated.[19] We therefore targeted the isolation of such compounds containing the Al(μ-O)**M** group to allow us to gain a better understanding of the bonding and to unequivocally demonstrate the viability of this pathway in our systems.

The reaction of **1-Zn** and **1-Mg** with $N_2O$ (1 bar) proceeded to afford (NON$^{Dipp}$)Al(μ-O)**M**(BDI$^{Mes}$) (**4-Zn** and **4-Mg**, Scheme 3). The $^1$H NMR resonances of the Si*Me*$_2$ groups are no longer broad (as noted for **1-Zn** and **1-Mg**), consistent with an increased distance between the NON$^{Dipp}$- and BDI$^{Mes}$-ligands and greater rotational freedom. X-Ray crystallography confirmed formation of the bimetallic complexes containing a μ-oxo ligand (Fig. 3). Each metal is three-coordinate, with an unsupported, approximately linear bridging oxo-ligand (Al–O–**M** range: 173.58(11)°–176.94(12)°). The Al–O bond lengths (range: 1.6413(16)–1.6472(15) Å) are considerably shorter than the sum of the molecular covalent double bond radii, $r_2$ ($\Sigma(r2)_{Al,O}$ = 1.70 Å) and almost indistinguishable from that noted in the terminal monoalumoxane anion, [Al(NON$^{Dipp}$)(O)]$^-$ (1.6362(14) Å).[18b] Significant differences are apparent when comparing the bonding in **4-Zn** and **4-Mg** with other Al(μ-O)**M** groups (**M** = Zn,[20] **M** = Mg[21]) involving tetrahedral Al.

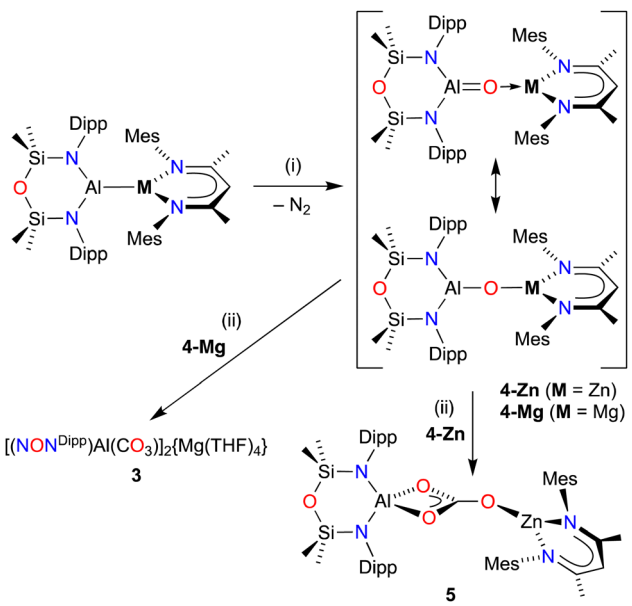


Scheme 3 Synthesis of **4-Zn**, **4-Mg** and **5**. (i) $N_2O$ (1 bar); (ii) $^{13}CO_2$ (1 bar).

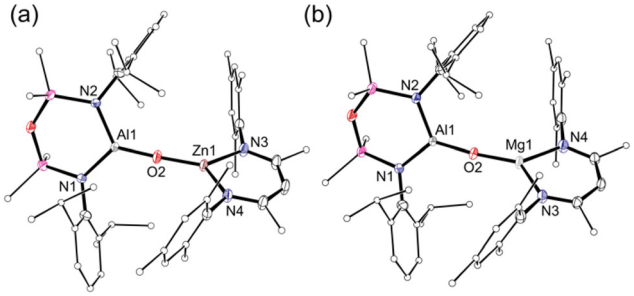


Fig. 3 Thermal displacement plot (30% probability, H-atoms omitted, selected carbon atoms represented as spheres) of (a) **4-Zn** and (b) **4-Mg**. Selected bond lengths (Å) and angles (°) {value from second molecule}: (a) Al1–O2 1.6413(16) {1.6428(15)}, Zn1–O2 1.7826(15) {1.7867(15)}; Al1–O2–Zn1 176.94(12) {173.74(11)}. (b) Al1–O2 1.6472(15) {1.6426(17)}, Mg1–O2 1.8004(16) {1.8009(18)}; Al1–O2–Mg1 173.58(11) {174.41(14)}.

In previous examples, the Al–O bond is longer (range: 1.671(2)–1.682(2) Å) with a significant bending at the μ-oxide atom (Al–O–**M** range: 144.78(15)°–159.6(1)°). These variations prompted a computational investigation of the electronic structure of the Al(μ-O)**M** group in **4-Zn** and **4-Mg**.

QTAIM and NBO analyses were performed at the BP86/BS2 level on **4-Zn** and **4-Mg** to interrogate the Al–O and O–**M** bonds. For both complexes, NBO7 charges show that the Al centre was more electropositive than **M**, although this charge difference was more notable for **4-Zn** ($\Delta q$ = +0.596) than **4-Mg** ($\Delta q$ = +0.400). QTAIM analysis identifies appreciable and similar Al–O bond critical points (BCPs) for each complex ($\rho(r)$: **4-Zn** = 0.101 *e*Å$^{-3}$; **4-Mg** = 0.104 *e*Å$^{-3}$), where positive Laplacian values ($\nabla^2\rho(r)$: **4-Zn** = 0.858 *e*Å$^{-5}$; **4-Mg** = 0.875 *e*Å$^{-5}$) and weakly positive energy densities, H(r), and $|V(r)| < 2G(r)$,[22] indicate an Al–O bond with ionic character in both complexes (Table S5, ESI†). This is further supported by low WBI$_{(Al-O)}$ values (**4-Zn** = 0.372; **4-Mg** = 0.426) when compared with the [Al(NON$^{Dipp}$)(O)]$^-$ anion (WBI$_{(Al-O)}$ = 1.11).[23] Moreover, we note that the values of $\rho(r)$ are similar to that of the monomeric [Al(NON$^{Dipp}$)(O)]$^-$ anion ($\rho(r)$ = 0.115 *e*Å$^{-3}$; $\nabla^2\rho(r)$ = 0.990 *e*Å$^{-5}$),[23] indicating that the terminal **M**(BDI$^{Mes}$) group only minimally perturbs the charge density and electronic composition of the Al–O bond. A more pronounced difference is observed for the O–**M** BCPs in each compound. For **4-Zn**, the O–Zn bond has more electron density at the BCP ($\rho(r)$ = 0.116 *e*Å$^{-3}$) than the adjacent Al–O BCP with a delocalization index DI(Zn|O) = +0.710 compared with DI(Al|O) = +0.404, suggesting the interaction is less ionic than Al–O. For **4-Mg**, however, a much lower density is captured at the O–Mg BCP ($\rho(r)$ = 0.066 *e*Å$^{-3}$), with a DI(Mg|O) = +0.270.

NBO analysis of **4-Zn** and **4-Mg** support the QTAIM analyses. Firstly, the NBO search in each complex generated an optimal Lewis structure essentially consisting of a series of 2s and 2p$_n$ lone pairs on a μ-oxo ion. Subsequent second-order perturbation energy analysis of the Fock matrix in the NBO basis reveals that the Al–O interaction consists of a suite of appreciable O → Al donor–acceptor NBO interactions, in which the 2s and 2p$_n$ donor NBOs on the bridging μ-oxo ion (LP$_{2px}$, LP$_{2py}$, LP$_{2pz}$) interact with vacant 3s and 3p$_n$ acceptor NBOs at the Al centre. Moreover, the

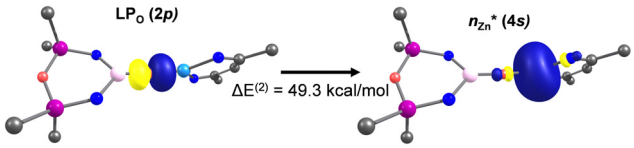


Fig. 4 The strongest donor–acceptor interaction between the bridging oxo and Zn identified *via* NBO in **4-Zn**.

O–**M** interaction is identified to be much stronger in **4-Zn** than **4-Mg**, with a significant O → Zn donor–acceptor interaction of $\Delta E^{(2)}\left[\mathrm{LP_O} \rightarrow n^*_{\mathrm{Zn}}\right]$ = 49.3 kcal mol$^{-1}$ (Fig. 4).

Conversion of the dioxocarbene ($_{\mathrm{xanth}}$NON$^{\mathrm{Dipp}}$)Al(μ-O$_2$C)**M**(P*t*Bu$_3$) to the carbonate species occurs under an atmosphere of $CO_2$ at −78 °C (**M** = Cu) or 80 °C (**M** = Ag), whereas the Al/Au analogue is stable.[10c] The (NC$_2$N$^{\mathrm{Dipp}}$) analogues were less reactive, with the corresponding Al(μ-O$_2$C)Cu requiring heating to 60 °C.[10d] To investigate this rection with our systems, a solution of **2** was heated to 353 K under an atmosphere of $^{13}CO_2$. However, no further reaction was noted, potentially reflecting the high carbophilicity of zinc. In contrast, a solution of the μ-oxide complex **4-Zn** reacted instantly with $^{13}CO_2$ to afford the carbonate product, (NON$^{\mathrm{Dipp}}$)Al(μ-CO$_3$)Zn(BDI$^{\mathrm{Mes}}$) (**5**). $^{13}C\{^1H\}$ NMR spectroscopy supports the formation of the carbonate product ($\delta_C$ 168.4) and a X-ray diffraction study confirms a 1κ$^2$O,O′:2κO″-bridging mode (Fig. S29, ESI†). These observations suggest the loss of CO from **2** to form **4-Zn** is energetically disfavoured, although addition to the μ-oxide to form the carbonate is a low energy process. The corresponding reaction of the magnesium complex **4-Mg** with $CO_2$ gave the carbonate product **3**.

In summary, we have shown that isolated Al(μ-O)**M** species react with $CO_2$ to form the carbonate product, confirming their role as intermediates in this reaction sequence.

M. P. C. and M. J. E. acknowledge Government funding from the Marsden Fund Council from, managed by Royal Society Te Apārangi (Grant Number: MFP-VUW2020). C. L. M. and S. E. N. acknowledge funding from the EPSRC (EP/R020752). This research made use of the Anatra, Balena (Bath) and Rāpoi (VUW) High Performance Computing (HPC) Services. Data used within this publication can be accessed from the Research Data Service – **https://library.bath.ac.uk/research-data**.

## Conflicts of interest

There are no conflicts to declare.

## Notes and references

1 (*a*) J. M. Gil-Negrete and E. Hevia, *Chem. Sci.*, 2021, **12**, 1982–1992; (*b*) T. X. Gentner and R. E. Mulvey, *Angew. Chem., Int. Ed.*, 2021, **60**, 9247–9262; (*c*) J. Campos, *Nat. Rev. Chem.*, 2020, **4**, 696–702; (*d*) S. D. Robertson, M. Uzelac and R. E. Mulvey, *Chem. Rev.*, 2019, **119**, 8332–8405.
2 I. G. Powers and C. Uyeda, *ACS Catal.*, 2017, **7**, 936–958.
3 (*a*) E. Bodio, M. Picquet and L. Gendre, in *Topics in Organometallic Chemistry*, ed., P. Kalck, Springer International Publishing, Switzerland, 2016, vol. 59, pp. 139–186; (*b*) N. Wheatley and P. Kalck, *Chem. Rev.*, 1999, **99**, 3379–3420.
4 X. Wang, C. Xia and L. Wu, *Green Chem.*, 2018, **20**, 5415–5426.
5 (*a*) M. Cokoja, C. Bruckmeier, B. Rieger, W. A. Herrmann and F. E. Kühn, *Angew. Chem., Int. Ed.*, 2011, **50**, 8510–8537; (*b*) X. Yin and J. R. Moss, *Coord. Chem. Rev.*, 1999, **181**, 27–59; (*c*) W. Leitner, *Coord. Chem. Rev.*, 1996, **153**, 257–284.
6 J. Hicks, P. Vasko, J. M. Goicoechea and S. Aldridge, *Angew. Chem., Int. Ed.*, 2021, **60**, 1702–1713.
7 J. Hicks, P. Vasko, J. M. Goicoechea and S. Aldridge, *Nature*, 2018, **557**, 92–95.
8 R. J. Schwamm, M. P. Coles, M. S. Hill, M. F. Mahon, C. L. McMullin, N. A. Rajabi and A. S. S. Wilson, *Angew. Chem., Int. Ed.*, 2020, **59**, 3928–3932.
9 M. M. D. Roy, J. Hicks, P. Vasko, A. Heilmann, A.-M. Baston, J. M. Goicoechea and S. Aldridge, *Angew. Chem., Int. Ed.*, 2021, **60**, 22301–22306.
10 (*a*) J. Hicks, A. Mansikkamäki, P. Vasko, J. M. Goicoechea and S. Aldridge, *Nat. Chem.*, 2019, **11**, 237–241; (*b*) H.-Y. Liu, R. J. Schwamm, M. S. Hill, M. F. Mahon, C. L. McMullin and N. A. Rajabi, *Angew. Chem., Int. Ed.*, 2021, **60**, 14390–14393; (*c*) C. McManus, J. Hicks, X. Cui, L. Zhao, G. Frenking, J. M. Goicoechea and S. Aldridge, *Chem. Sci.*, 2021, **12**, 13458–13468; (*d*) H.-Y. Liu, S. E. Neale, M. S. Hill, M. F. Mahon and C. L. McMullin, *Dalton Trans.*, 2022, **51**, 3913–3924.
11 (*a*) C. Weetman, A. Porzelt, P. Bag, F. Hanusch and S. Inoue, *Chem. Sci.*, 2020, **11**, 4817–4827; (*b*) C. Weetman, P. Bag, T. Szilvási, C. Jandl and S. Inoue, *Angew. Chem., Int. Ed.*, 2019, **58**, 10961–10965; (*c*) J. A. Castro-Osma, M. North, W. K. Offermans, W. Leitner and T. E. Müller, *ChemSusChem*, 2016, **9**, 791–794.
12 R. J. Schwamm, M. D. Anker, M. Lein and M. P. Coles, *Angew. Chem., Int. Ed.*, 2019, **58**, 1489–1493.
13 (*a*) C. Bakewell, B. J. Ward, A. J. P. White and M. R. Crimmin, *Chem. Sci.*, 2018, **9**, 2348–2356; (*b*) S. Brand, H. Elsen, J. Langer, S. Grams and S. Harder, *Angew. Chem., Int. Ed.*, 2019, **58**, 15496–15503; (*c*) A. Paparo, C. D. Smith and C. Jones, *Angew. Chem., Int. Ed.*, 2019, **58**, 11459–11463; (*d*) A. Friedrich, J. Eyselein, J. Langer, C. Färber and S. Harder, *Angew. Chem., Int. Ed.*, 2021, **60**, 16492–16499.
14 J. Weßing, C. Göbel, B. Weber, C. Gemel and R. A. Fischer, *Inorg. Chem.*, 2017, **56**, 3517–3525.
15 To examine the factors that determine the charges calculated for Al–M systems, a more detailed study is underway investigating the role of different levels of theory and QC charge schemes on the computed values.
16 (*a*) P. Jochmann and D. W. Stephan, *Chem. – Eur. J.*, 2014, **20**, 8370–8378; (*b*) M. E. Grundy, K. Yuan, G. S. Nichol and M. J. Ingleson, *Chem. Sci.*, 2021, **12**, 8190–8198.
17 S. J. Bonyhady, C. Jones, S. Nembenna, A. Stasch, A. J. Edwards and G. J. McIntyre, *Chem. – Eur. J.*, 2010, **16**, 938–955.
18 (*a*) J. Hicks, A. Heilmann, P. Vasko, J. M. Goicoechea and S. Aldridge, *Angew. Chem., Int. Ed.*, 2019, **58**, 17265–17268; (*b*) M. D. Anker and M. P. Coles, *Angew. Chem., Int. Ed.*, 2019, **58**, 18261–18265.
19 The reaction of ($_{\mathrm{xanth}}$NON$^{\mathrm{Dipp}}$)Al–Ag(P*t*Bu$_3$) with $N_2O$ generated the μ-O bridged species in situ. However the complex proved "too thermally fragile to be isolated". See reference 10(c).
20 S. Schulz, J. Spielmann, D. Bläser and C. Wölper, *Chem. Commun.*, 2011, **47**, 2676–2678.
21 (*a*) S. Nembenna, H. W. Roesky, S. K. Mandal, R. B. Ostwald, A. Pal, R. Herbst-Irmer, M. Noltemeyer and H.-G. Schmidt, *J. Am. Chem. Soc.*, 2006, **128**, 13056–13057; (*b*) S. Nembenna, S. Singh, S. S. Sen, H. W. Roesky, H. Ott and D. Stalke, *Z. Anorg. Allg. Chem.*, 2011, **637**, 201–205.
22 P. S. V. Kumar, V. Raghavendra and V. Subramanian, *J. Chem. Sci.*, 2016, **128**, 1527–1536.
23 M. J. Evans, M. D. Anker, C. L. McMullin, S. E. Neale, N. A. Rajabi and M. P. Coles, *Chem. Sci.*, 2022, **13**, 4635–4646.